Journal of Applied Fluid Mechanics, Vol. 14, No. 4, pp. 1053-1063, 2021.
Available online at www.jafmonline.net, ISSN 1735-3572, EISSN 1735-3645.
https://doi.org/10.47176/jafm.14.04.31846

Research on the Characteristics of Bluff Body Wake Field Induced by Synthetic Jet with PANS Model

Z. Hao[1,2,3], G. Liu[1,2,3†], W. Ren[1,2,3], Y. Wang[1,2,3] and H. Bie[4]

[1] *Institute of Oceanographic Instrumentation, Qilu University of Technology (Shandong Academy of Sciences), Qingdao, 266100, China*
[2] *Shandong Provincial Key Laboratory of Marine monitoring instrument equipment technology, Qingdao, 266100, China*
[3] *National Engineering and Technological Research Center of Marine Monitoring Equipment, Qingdao, 266100, China*
[4] *College of Chemistry and Chemical Engineering, Ocean University of China, Qingdao 266100, China*

†*Corresponding Author Email: liu-g@qlu.edu.cn*

(Received May 19, 2020; accepted December 4, 2020)

ABSTRACT

Based on the active control theory, the synthetic jet behind the blunt body is explored by considering the control of flow around the blunt body in this paper. The Partially Averaged Navier-Stokes model was carried out for flow around circle cylinder at two subcritical Reynolds numbers (*Re*=1000, 3900), whose results have a good agreement with the experimental data. The results indicate that synthetic jet behind the circle cylinder has essential effects on the vortex shedding of flow around circle cylinder. The analysis of the Vorticity and Q vortex shows that the increasing velocity of synthetic jet has a strong effect on the vortex shedding of the original flow field. It is noted that the information including the coherence data and the directivity pattern with the existence of synthetic jet is different from that without synthetic jet. These results imply that the synthetic jet in the tail of the blunt body could control the flow fields around the blunt body.

Keywords: Flow around circle cylinder; PANS model; Vortex shedding; Synthetic jet; Noise control.

NOMENCLATURE

Nomenclature should be in alphabetic order (A – Z) and Greek letters should follow after Latin letters in alphabetic *order (α β ...)*

Cl	lift coefficient of cylinder	*P*	pressure
Cd	drag coefficient of cylinder	*PSD*	power spectrum density
Cp	pressure coefficient of cylinder	*SPL*	sound pressure level
d	the diameter of cylinder	*St*	Strouhal number
f	frequency		
h	the width of gap	*ρ*	density
l	central distance of vortex	*γ*	coherence coefficient

1. INTRODUCTION

In modern practical engineering, the condition of flow around blunt body plays a pivotal role in various offshore structures, ocean structures and aviation industries (Anibal 2018, Paul and Tiwari 2019). It is essential to comprehend the mechanisms of the flow around the blunt body to control the dynamical responses, even the acoustic information. The computational fluid dynamic method has been widely utilized by scholars to calculate the information of flow mechanisms. In order to obtain the detailed information of flow filed, a proper turbulence model is required.

The accuracy of the flow calculation plays an important role in the simulation. In order to achieve higher precision calculations, based on the variable filtering model proposed by Speziale (1997). Girimaji proposed a bridging model, i.e. Partially Averaged Navier-Stokes (*PANS*) whose accuracy is

between *RANS* and DNS, which is different from URANS (Girimaji *et al.* 2003, Chaouat 2010, Arwatz *et al.* 2012). Low Reynolds number flow simulated by the original PANS model could agree well with the experimental data by Lakshmipathy and Girimaji (2006). Based on *k*-*ω* model and *k*-*ε* model, Davidson and Peng (2013) developed *k*-*ω* PANS and *k*-*ε*-*ξ*-*f* PANS that could improve the accuracy of near-wall flow field. Shur *et al.* (2011) improved the *PANS* model based on the LES model. According to the work of these scholars, the unresolved-to-total ratio of kinetic energy f_k and the unresolved-to-total ratio of dissipation f_ε of the *PANS* model would play a critical role to the simulation accuracy of the flow field, especially for low Reynolds number flow. The present work would discuss how wide range of f_k affects flow result in details, and compares with the experiment result of Norberg (1998) and Lourenco (1993).

Noise control techniques of flow around circle cylinder can be classified into passive control and active control, whether there is energy supply as distinguish criterion (Zdravkovich 1981). You and Moin (2007) modified the cylinder surface. Then it is concluded that vortex shedding has been changed with altering flow structure. Strykowski and Sreenivasan (1990) and Wang *et al.* (2006)studied the variations of lift and drag by putting a small blunt body in the cylinder flow wake. Wang *et al.* (2006) assessed the effectiveness of attached permeable plates in suppressing vortex shedding from a cylinder. There is no energy injection in these ways, which can still cause noise impact.

Active control needs external energy input which has different forms such as acoustic waves, plasma, heat and magnetism. Yahiaoui *et al.* (2015) used moving surface boundary layer control to suppress vortex shedding of flow around circle cylinder. J.H.M. Arwatz *et al.* (2012) utilized blowing and suction function to change the lift force coefficients. Sen *et al.* (2016) altered the primitive flow field by setting injected jets in the opposite flow direction of cylinder body. Kou *et al.* (2017) developed a modeling method for unstable flow with oscillating shock waves and moving boundaries based on active control. However, the above researches focused on focused on the influence of synthetic jet to the flow around blunt body.

In this paper, a synthetic jet behind the cylinder body is introduced to control both the flow and acoustics fields. The presence of perturbations caused by the synthetic jet is observed in wake of cylinder flow, and then the perturbation transforms the flow structure and reduces the sound pressure level that based on synthetic jet. Section 2 described briefly the *PANS* model and Lighthill acoustic analogy theory. The physical model, numerical simulation method and mesh generation are presented in detail in Section 3. Section 4 is main part of this paper which discusses the flow field of cylinder flow at *Re*=1000 and *Re*=3900. The flow field is analyzed by vorticity, *Q* criterion, and acoustic field information is explained by the coherence analysis, spectrum analysis, and directivity analysis method.

2. DESCRIPTION OF THEORETICAL METHODOLOGY

The hybrid method that combined Lighthill acoustic analogy and flow simulation is the common way to research the acoustic prediction by many investigators. In this work, PANS model is used to simulate the flow around blunt body. The analysis of noise should be on the basis of the pressure pulsation and velocity pulsation of flow field. Therefore, the transient flow field of physical model should be simulated firstly. Then, equivalent sound source would be obtained by the way of using Lighthill acoustic analogy to transform the transient flow field of physical model.

2.1 *PANS* Model

The modified *PANS* linear model is employed to simulate the cylinder flow based on the standard *k*-*ε* model in this work. All variables would adhere the rules that the fluctuating part of the quantities are denoted with upper corner mark"’" while the averaged parts of the quantities are denoted with upper mark “-”.

The turbulence kinetic energy *k*, and the turbulence dissipation *ε*, are obtained from the following incompressible transport equations:

$$\frac{\partial(\rho k)}{\partial t}+\frac{\partial\left(\rho\overline{U}_j k\right)}{\partial x_j}= \frac{\partial}{\partial x_j}\left[(\mu+\frac{\mu_t}{\sigma_k})\frac{\partial k}{\partial x_j}\right] +P_k-\rho\varepsilon \tag{1}$$

$$\frac{\partial(\rho\varepsilon)}{\partial t}+\frac{\partial\left(\rho\overline{U}_j \varepsilon\right)}{\partial x_j}= \frac{\partial}{\partial x_j}\left[(\mu+\frac{\mu_t}{\sigma_\varepsilon})\frac{\partial \varepsilon}{\partial x_j}\right] +C_{\varepsilon 1}P_k\frac{\varepsilon}{k}-C_{\varepsilon 2}\rho\frac{\varepsilon^2}{k} \tag{2}$$

where ρ denotes the fluid density, μ_t denotes the turbulence viscosity coefficient, and P_k denotes the generation of turbulence kinetic energy which is calculated by:

$$P_k=-\rho\overline{U_i'U_j'}\frac{\partial\overline{U}_i}{\partial x_j} \tag{3}$$

Other constant number are given as:$C_{\varepsilon 1}$=1.44, $C_{\varepsilon 2}$=1.92, σ_k=1.0, σ_ε=1.3.

As the employed *PANS* model is based on the stand *k*-*ε* model, the unresolved-to-total ratio of kinetic energy f_k and the unresolved-to-total ratio of dissipation f_ε are acquired from the following equations:

$$\frac{\partial(\rho k_u)}{\partial t}+\frac{\partial\left(\rho u_j k_u\right)}{\partial x_j}= \frac{\partial}{\partial x_j}\left[(\mu+\frac{\mu_t}{\sigma_{ku}})\frac{\partial k_u}{\partial x_j}\right]+P_{ku}-\rho\varepsilon_u \tag{4}$$

$$\frac{\partial(\rho\varepsilon_u)}{\partial t}+\frac{\partial(\rho u_j\varepsilon_u)}{\partial x_j}= \frac{\partial}{\partial x_j}\left[(\mu+\frac{\mu_t}{\sigma_{\varepsilon u}})\frac{\partial\varepsilon_u}{\partial x_j}\right]+ C_{\varepsilon 1}P_{ku}\frac{\varepsilon_u}{k_u}-C^*_{\varepsilon 2}\rho\frac{\varepsilon_u^2}{k_u} \tag{5}$$

where k_u is the sub-filter kinetic energy and ε_u is the dissipation. v_u is turbulent viscosity coefficient and S_{ij} is deformation tensor. These parameters could be obtained by:

$$k_u=\frac{1}{2}\tau(V_i,V_j) \tag{6}$$

$$\varepsilon_u=v\tau\left(\frac{\partial V_i}{\partial x_j},\frac{\partial V_j}{\partial x_i}\right) \tag{7}$$

$$\tau(V_i,V_j)=-v_u S_{ij} \tag{8}$$

$$v_u=C_\mu\frac{k_u^2}{\varepsilon_u} \tag{9}$$

$$S_{ij}=\frac{1}{2}\left(\frac{\partial U_i}{\partial x_j}+\frac{\partial U_j}{\partial x_i}\right) \tag{10}$$

Then the unresolved-to-total ratio of kinetic energy f_k is written as:

$$f_k=\frac{k_u}{k} \tag{11}$$

The unresolved-to-total ratio of dissipation f_ε is written as:

$$f_\varepsilon=\frac{\varepsilon_u}{\varepsilon} \tag{12}$$

The Prandtl number of unresolved kinetic energy σ_{ku}, and the Prandtl number of unresolved kinetic energy dissipation $\sigma_{\varepsilon u}$ are acquired as follows:

$$\sigma_{ku}=\sigma_k\frac{f_k^2}{f_\varepsilon},\qquad \sigma_{\varepsilon u}=\sigma_\varepsilon\frac{f_k^2}{f_\varepsilon} \tag{13}$$

The dissipation factor $C_{\varepsilon 2}^*$ is written as:

$$C^*_{\varepsilon 2}=C_{\varepsilon 1}+\frac{f_k}{f_\varepsilon}(C_{\varepsilon 2}-C_{\varepsilon 1}) \tag{14}$$

The parameter P_{ku} in Eq. (4) and Eq. (5) is the production term, which is expressed by:

$$P_{ku}=f_k(P_k-\varepsilon)+\varepsilon_u \tag{15}$$

The Reynolds stress P_k in Eq. (1) is based on the incompressible *RANS* linear model, which is calculated by:

$$P_k=\mu_t\left(\frac{\partial U_i}{\partial x_j}+\frac{\partial U_j}{\partial x_i}\right)\frac{\partial U_i}{\partial x_j} \tag{16}$$

2.2 Acoustic Analogies

Based on the analysis of flow field, the acoustic simulation is introduced. Lighthill has suggested an inhomogeneous wave equation of acoustic analogy, having the source derived by comparing the exact equations of motion of a fluid with the equations of sound propagation in a medium at rest as follows (Lighthill, 1954). The sound propagation is governed by the equations from the Lighthill acoustic analogy as follows:

$$\frac{\partial^2\rho'}{\partial t^2}-c_0^2\nabla^2\rho'=\frac{\partial^2 T_{ij}}{\partial x_i\partial x_j} \tag{17}$$

$$T_{ij}=\rho u_i u_j+\left(p_{ij}-\rho c_0^2\right)\delta_{ij}-\sigma_{ij} \tag{18}$$

where, $\rho'=\rho-\rho_0$ is the density perturbation, T_{ij} is Lighthill's stress tensor, p_{ij} is compressive stress tensor, c_0 is velocity of sound in fluid at rest.

In the present work, considering a compact body (i.e. the cylinder) set in the flow, the free-field Green's function is used to solve Lighthill's equations by Curle (Lyu *et al.* 2017). As the length scale of the body is very small compared to the wave length, the sound source is assumed compact. In the case of a compact, fixed, and rigid body, emission time variation along the body can be neglected. Hence, $r\approx|x|$. Therefore, this paper takes *Pij* as pressure, and instantaneous force F_i of fluid on the body (i.e. lift and drag) as:

$$F_i(t_r)\approx\int_S\left[P_{ij}\right]_{\tau=t_r}n_j dS(y) \tag{19}$$

Where, t_r is the radial vector, n_j is normal vector, dS is the integration surface.

The Curle's solution for a fixed rigid compact body is

$$c_0^2\left[\rho(x,t)-\rho_0\right]=\frac{1}{4\pi r^2}\frac{x_i x_j}{rc_0^2}\int_V T_{ij}(y,t-r/c_0)dV(y) -\frac{1}{4\pi r^2}\frac{x_j}{c_0^3}\frac{\partial}{\partial t}F_j(t-r/c_0) \tag{20}$$

Where, r is the distance between monitoring point and sound source, x is the coordinates of monitoring points, y as the point on the rigid surface.

Hence, the radiated sound is calculated from quadruple volume integration and a dipole surface integration. As Inoue estimated that $p'_q/(\rho U_\infty^2)\propto AMa^{7/2}/r^{1/2}$ and $p'_d/(\rho U_\infty^2)\propto AMa^{7/2}/r^{1/2}$, where subscripts '*q*' and '*d*' are for quadruple and dipole respectively. However, the quadruple contribution is usually small compared to the dipole contribution (Williams Ffowcs 1974). So the quadruple is neglected in this study.

3. Numerical Method And PANS Calculation

A general purposed CFD software Fluent was

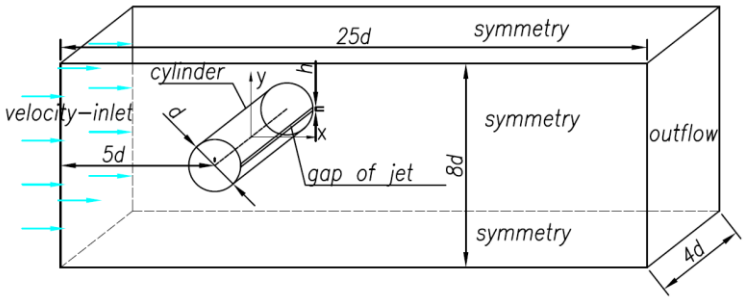

Fig. 1. Illustration of computation domain.

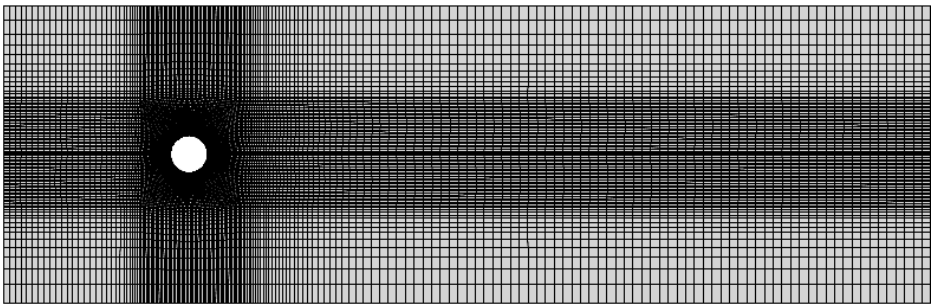

Fig. 2. Cross-section mesh.

employed to simulate the unsteady flow around the cylinder in this study. The computational solver is a finite volume pressure-based method (Wilcox *et al.* 2003). The pressure-based solvers are typically used for low speed incompressible flows which is proper for this study. The numerical procedure is based on an implicit, fractional step technique with a pressure Poisson solver. A 2nd order upwind scheme is available for temporal discretization, which was used by many researchers such as Samulyak *et al.* (2016). The discretization of momentum, turbulent kinetic energy and turbulent dissipation rate also adopt 2nd order upwind (Rubel 1985).

The computational domain of flow around cylinder is illustrated in Fig.1. The origin of the coordinate system is the center of the cylinder. The top and bottom boundaries of the domain are placed at 4d from the cylinder axis, with d representing the diameter of the cylinder. The upstream inlet and the downstream outlet are located at 5d upstream and 20d downstream from the cylinder center, respectively. The spanwise distance of computation domain is 4d.

On the cylinder wall, y^+ of cylinder wall is small enough($0<y^+<0.7$) for the cases computed in this study, and the pattern of mesh generation adopts structured grid. The boundary condition of the cylinder is set as no slip wall condition. Inlet and outlet sections are illustrated as Fig.1, in which the velocity-inlet is described with a uniform velocity, and the outlet boundary condition is set as outflow. The inlet of synthetic jet is set as velocity-inlet which located in the gap of inlet. And other sides of computation domain are set as symmetry to keep cylinder flow free from boundary influence in Fig.1.

The mesh of the computational domain is shown in Fig.2.

Computation of the flow around the cylinder at *Re*=1000 and *Re*=3900 were carried out. The velocity value of different Re number is 0.1m/s and 0.39m/s. The energy of synthetic jet behind cylinder can be characterized by jet velocity. The velocity of synthetic jet could be set as *0.5v*, *v*, *2v*, *3v*, *4v*, *5v*, and the width of jet gap h satisfies *h/d*=0.05, with h representing the distance of gap of the jet. And the diameter of cylinder is kept the same as cylinder without synthetic jet.

3.1 Grid Convergence Research

The grid convergence study was carried out by keeping progressively decreasing the grid size. Three kinds of mesh were conducted grid convergence study in domain for computational convergence at *Re*=3900. All kinds of mesh guaranteed the nearby mesh of cylinder satisfied $y+ \leqslant 1$. The results of three kinds of mesh which were computed by *PANS* model and the experiment values of Norberg (Norberg 1998) were listed in Tab.1. The results of *PANS* model fits well with the experiment values of Norberg (Norberg 1998) and Ong (Ong and Wallace 1996). The calculation accuracy changed little with increase of mesh quantity, and all information is listed in Tab.1. The mean *Cp* of different case is shown in Fig. 3. And the curve of Fig. 3 show that the result of case 3 is similar to the experiment value. Considering the computation time and effectiveness, it is feasible that Case 3 could be chosen to perform the following calculation of cylinder flow.

Table 1 Comparison of result with different mesh and experiment value

	Mesh number	*Cd*	*St*
EXP（*Norberg* 1987）		0.98	0.215
Case 1	600×250×40	1.01	0.21
Case 2	400×150×40	1.03	0.207
Case 3	300×110×40	1.05	0.206

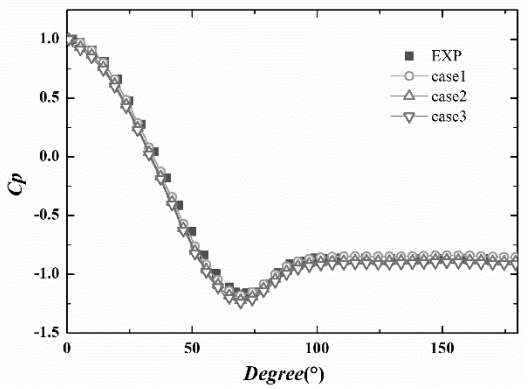

Fig. 3. Time-averaged *Cp* of different mesh at *Re*=3900.

3.2 Comparison of the Result of Cylinder Flow with Different Methods

The unresolved-to-total ratio of kinetic energy f_k is set as 0.2, 0.4, 0.6, 0.8 and 1.0 in the computation along with cylinder flow at *Re*=3900 and *Re*=1000. The time interval of computation is 0.001s, and eight hundred time interval was used to complete the mean time value for flow analysis. The detailed information of the comparison among the results of *PANS* model, and the experiment value of Norberg (Norberg 1998), Lourence (Lourenco 1993) and Ong *et al* (Ong and Wallace 1996) is shown in Figs.4~6.

The solution of resolve *Cp* and *Cl* is as follows:

$$C_p = \frac{P}{\frac{1}{2}\rho U^2 A} \tag{21}$$

$$C_l = \frac{F_l}{\frac{1}{2}\rho U^2 A} \tag{22}$$

Where, *A* is area of upstream section, *U* is inlet velocity, *P* is the pressure of cylinder body, ρ is density of water.

The mean pressure distribution on the cylinder surface compared with experimental value at *Re* = 1000 and *Re* = 3900 is illustrated in Fig. 4. A good agreement is observed between *PANS* model with f_k = 0.2 and the experiment of Norberg which is performed at *Re* = 3900 and *Re* = 1000. The result of *PANS* model provides a satisfactory agreement to experimental value while f_k distressed. A quantitative comparison between experimental data and *PANS* in terms of the mean velocity profiles in the cylinder wake is shown in Fig. 6-7. Figure 6 illustrates the power spectra of the normal velocity fluctuation at the location of *x/d* = 3 on the centerline of the wake.

It is found that the PANS model predicts pretty well and coincides with experiment value, about means velocity of *x/d*=0.58, 1.06 and power spectra of normal velocity fluctuations of *x/d*=3 at *Re*=3900, especially the results of *PANS* model with lower fk. This paper utilizes *PANS* model with f_k =0.2 to simulate the cylinder flow with synthetic jet.

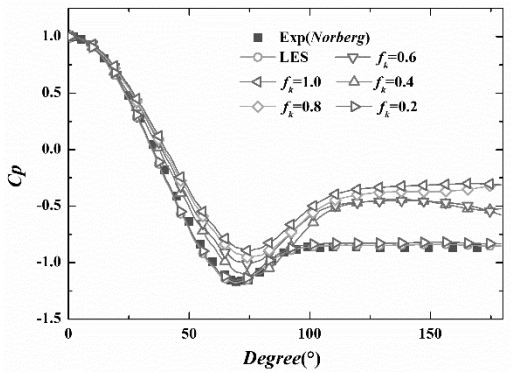

a) *Re*=3900

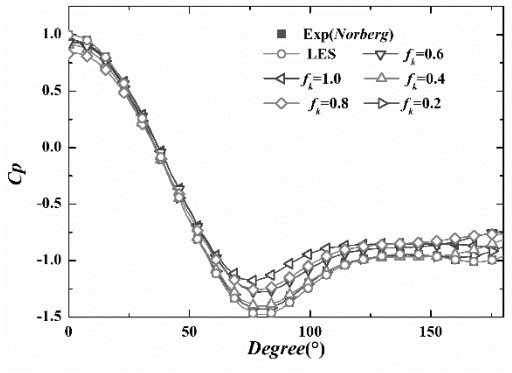

b) *Re*=1000

Fig. 4. Mean *Cp* of cylinder surface at *z*=0.

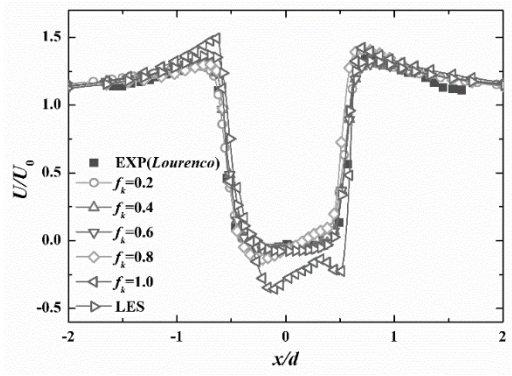

Fig. 5. *U/U0* at *x/d*=0.58.

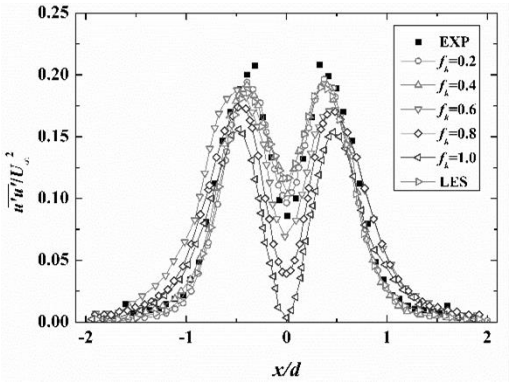

(a) $\overline{u'u'}/U^2$ at x/d=0.5

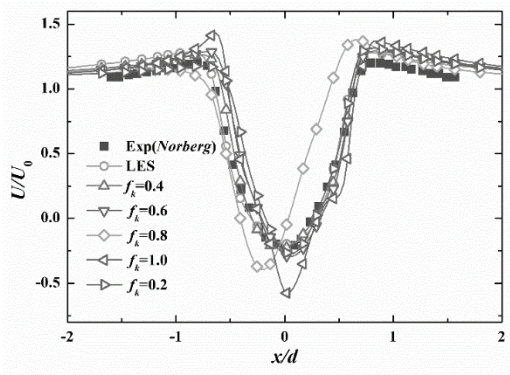

(b) U/U_0 at x/d=1.06

Fig. 6. Comparisons between the numerical calculation with experimental data ((a): Reynolds stress $\overline{u'u'}/U^2$ at x/d=0.5; (b): Velocity $U/U0$ at x/d=1.06).

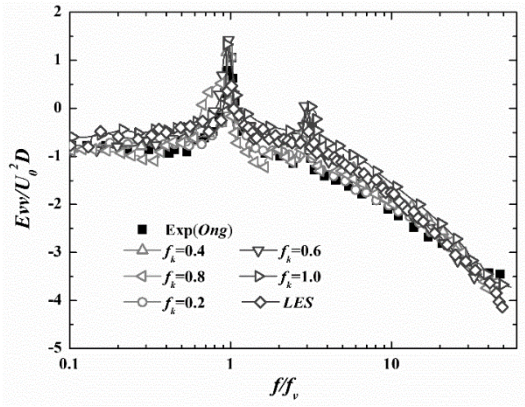

Fig. 7. Power spectra of the normal velocity fluctuations.

4. RESULTS AND DISCUSSION

Two classical conditions of cylinder flow are chosen as research conditions, and synthetic jet is set behind cylinder at Re=1000 and Re=3900. The *PANS* model with f_k=0.2 is applied for computing the flow field. The time interval of computation is 0.001s, eight hundred time interval was set to do the work of flow analysis and acoustic analysis in this section. According to flow field result, acoustic information of cylinder flow with jet can be obtained by Lighthill acoustic analogy. In this section, the information of cylinder flow without synthetic jet has a superscript "*org*" and the information of cylinder with synthetic jet has the superscripts including "0.5*v*", "*v*", "2*v*", "3*v*", "4*v*", "5*v*" which marked by synthetic jet velocity.

4.1 Flow Field Analysis

Vortex Analysis

The vortex contour of flow around cylinder with different synthetic jet is illustrated in Fig.8 (a represents org which cylinder flow wi*thout jet, while b-g represent the velocity from 0.5v* to 5*v*), which portray the structure of wake with different jet velocities for Re=3900 predicated by *PANS* model. The value of x direction of vortex was 100 as shown in Fig.8. In Fig.8, the vortex street is gradually disappearing while the velocity of synthetic jet gradually strengthening. From the contour, it is concluded that the shear action between jet and vortex street gradually strengthens and promotes the vortex to deform. The vorticity of the flow field with jet velocity at 4*v* and 5*v* is dominated by jet characteristic and controls the appearance of the vortex. These observations indicated that the synthetic jet can change the vortices shedding frequency.

Figure 9 and Fig.10 present qualitative differences of cylinder flow with various velocity of jet on the same boundary conditions at Re=1000 and Re=3900 respectively (a represents the Q contour of cylinder flow without synthetic jet (Jeong and Hussain 1995), b-g represent the Q contour of the cylinder flow with different synthetic jet velocity of 0.5*v*, *v*, 2*v*, 3*v*, 4*v*, 5*v*). The instantaneous contour for different jet velocity in computation domain is shown by the same value of Q which is set 100. The vorticity is displayed on the contour surface of instantaneous contour. The color of isosurface is velocity distribution in Fig. 9 and Fig. 10.

Although Reynolds number is different, Fig. 9 and Fig. 10 present the same phenomenon. Cylinder flow without jet has clear vortex tube that sheds with periodicity. The vortex tube has been diminished gradually while the velocity of jet increases in both cases (Fig. 9 and Fig. 10). When the velocity of jet is 4*v* or 5*v*, the main flow pattern of the fluid domain is dominated by synthetic jet, especially at 5*v*. The vortex street of cylinder flow is suppressed with the increase of jet velocity.

Coherence of *Cl* of cylinder Flow Without and with Synthetic Jet

The correlation between waves and other waves can be described by coherence. As mentioned above, the lift coefficient *Cl* is related to jet velocity, which means that it is able to use coherence to describe the relationship. The calculation method of coherence functions is given as follows:

$$\gamma_{xy} = \frac{\left|G_{xy}(f)\right|^2}{G_{xx}(f)G_{yy}(f)} \qquad (23)$$

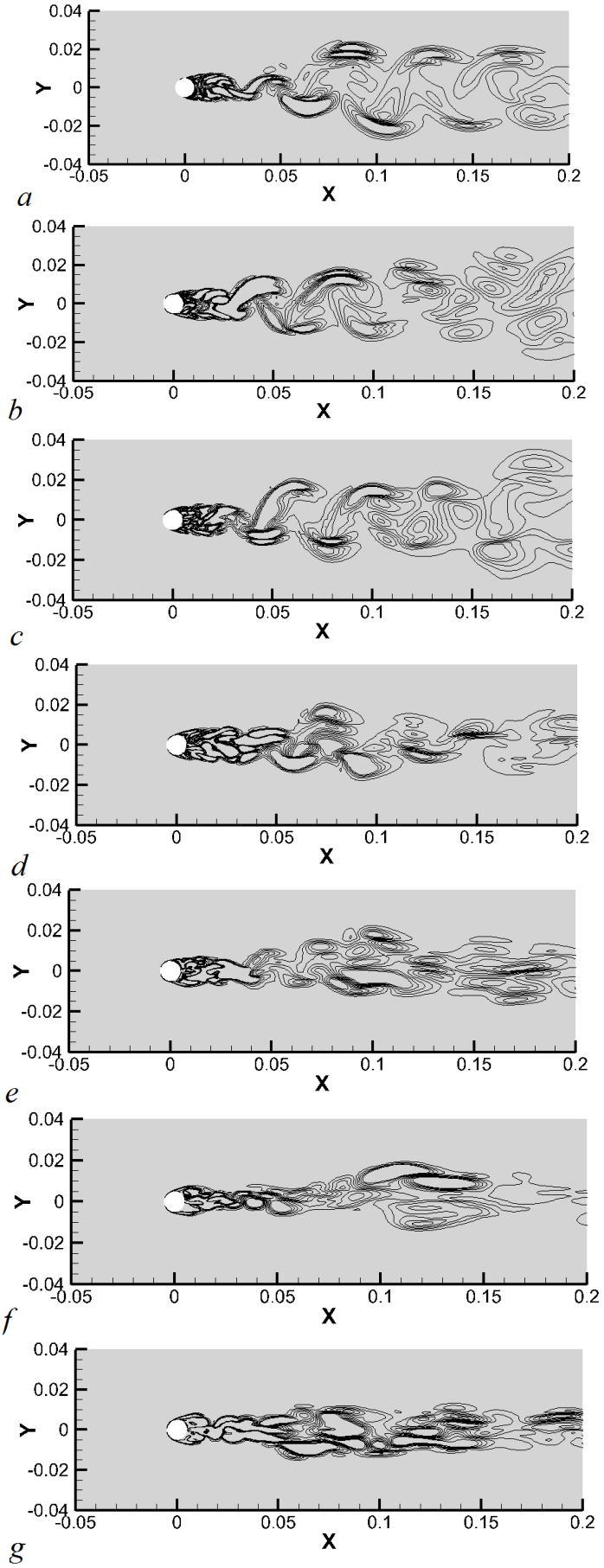

Fig. 8. Vorticity distribution at Re=3900.

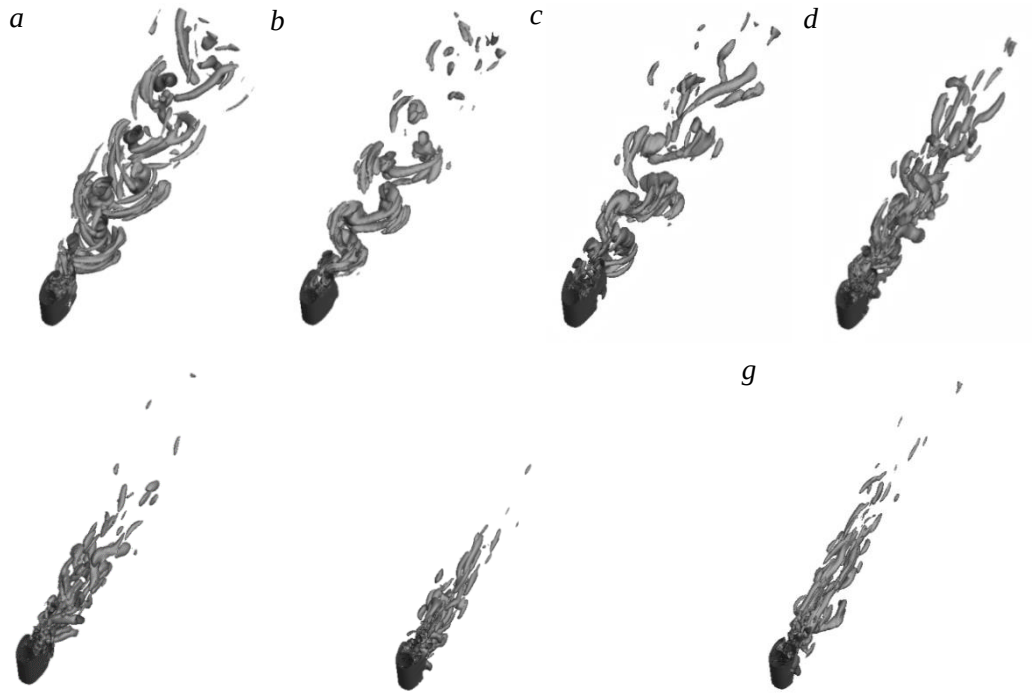

Fig. 9. Velocity distribution on the *Q* vortex at *Re*=1000 (*a*: flow without jet; *b-f*: flow with synthetic jet of 0.5*v*, *v*, 2*v*, 3*v*, 4*v*, 5*v*, respectively).

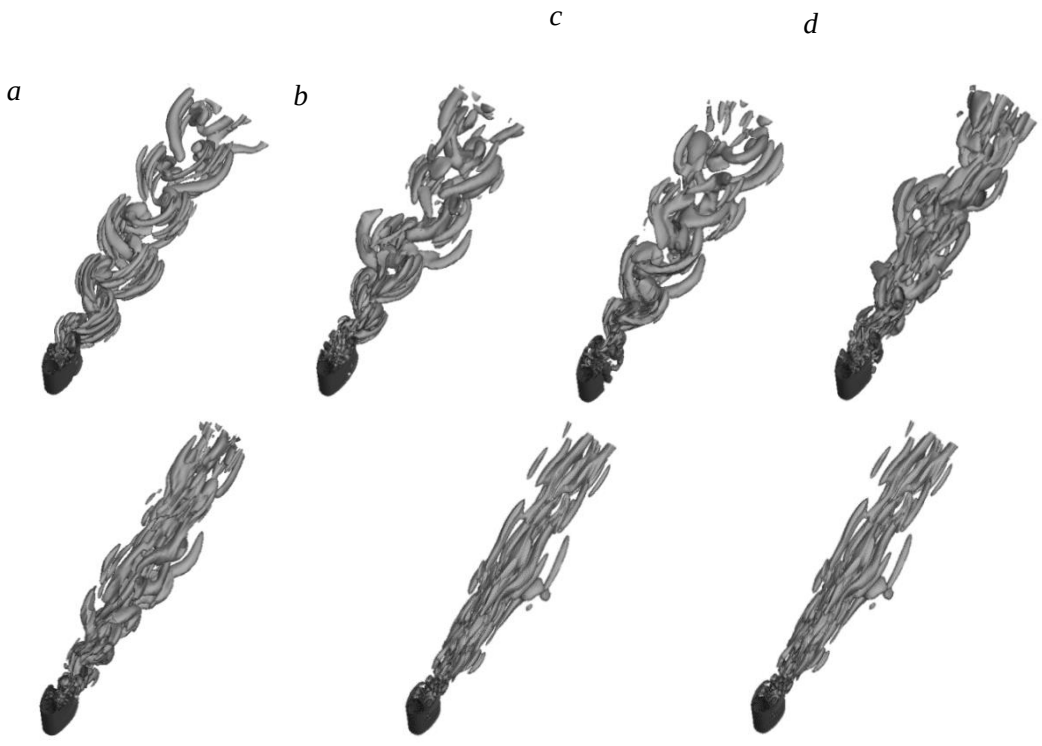

Fig. 10. Velocity distribution on the Q vortex at Re=3900 (*a*: flow without jet; *b-f*: flow with synthetic jet of 0.5*v*, *v*, 2*v*, 3*v*, 4*v*, 5*v*, respectively).

$$G_{xx}(f)=\sum_{m=0}^{\infty} r_x(m) r_x(m) e^{-jfm} \quad (24)$$

Where, G is the power spectral density function of signal; m is the number of discrete point, the computation method of G_{xy} and G_{yy} are as the same as the G_{xx}, $r_x(m)$ is the sequence of the signal x. The signal x or y represents the Cl of flow around blunt body at different case. γ=0 represents signal x and signal y is completely irrelevant, γ=1 represents

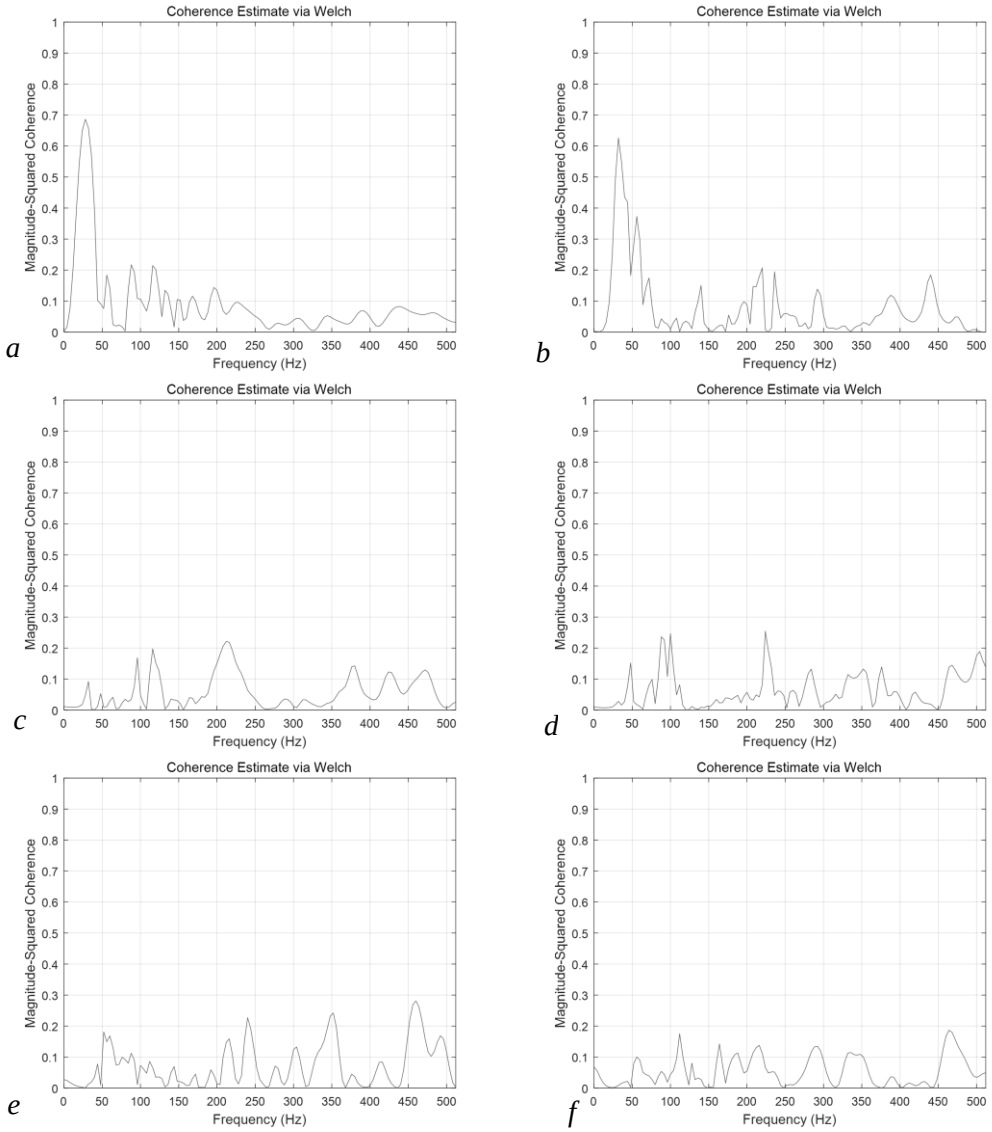

Fig. 11. Coherence of cylinder flow with various jet at *Re*=3900 (*a*: flow without jet; *b-f*: flow with synthetic jet of 0.5*v*, *v*, 2*v*, 3*v*, 4*v*, 5*v*, respectively).

signal *x* and signal *y* is completely relevant; in common situation, $0<\gamma<1$.

The lift coefficient *Cl* as the signal is chosen to explore the influence of synthetic jet on flow around blunt body. The coherence curve of flow around cylinder with different case at *Re*=3900 are illustrated respectively in Fig.11.

In Fig.11, the coherence signal of *Cl* of cylinder flow with 0.5*v* jet and cylinder flow without jet has peak value at low frequency. The peak value of coherence signal is closed to the peak frequency of *Cl* with the case of 'org' which indicated that these two cases have strong coherence. The signals of 'org' and 'v' also have coherence at low frequency which has lower coherence than 'org' and '0.5*v*'. As the velocity of jet increases, it is found that the signal lacks of coherence. It means that the synthetic jet has strong function to the flow around cylinder. The flow around cylinder with high synthetic jet is dominated by synthetic jet. The coherence of different case has good agreement with the vortex analysis and *PSD* analysis. In summary, the synthetic jet with high energy has great impact to flow around cylinder from the perspective of flow.

4.2 Acoustic Analysis

The acoustic computation was based on the Acoustic Analogies in section 2.2. The computation of acoustic was done after flow computation. The number of time interval was eight hundred.

Figure 12 presents the variations of acoustic directivity curve for 20*d* field point at *Re*=1000 and *Re*=3900. The subfigure *a* is *Re*=1000.It could be observed that the sound pressure level decreases while the velocity of jet increases. The directivity curves with different jet velocities have the same trend with peak frequency of acoustic spectrum analysis. And this phenomenon also meets the vortex

distribution in Fig.9. The flow field of cylinder flow has been changed by synthetic jet. The directivity curve displays '8' shape coincide with dipole source. And as the synthetic jet increases, the directivity curve '8' shape becomes unclear. It means that the acoustic source is not dominant by dipole source. The effect of synthetic jet has been the new acoustic source.

Another comparison of sound pressure level at *Re*=3900 is illustrated subfigure b. The variations of directivity curve varying with the velocity of jet are consistent with the trend in Fig.12. The change in the trend of directivity curve shape with different jet velocities is the same as the case at *Re*=1000. The directivity curve lost '8' shape when the synthetic jet velocity increases.

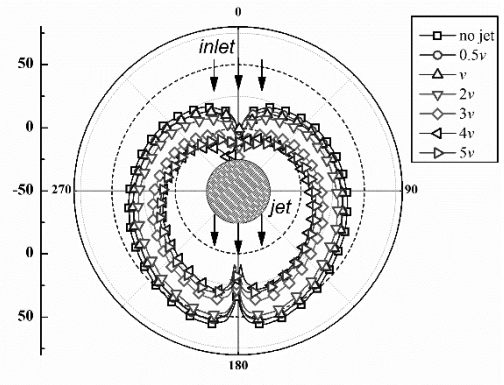

(a) Acoustic directivity of 20*d* at *Re*=1000

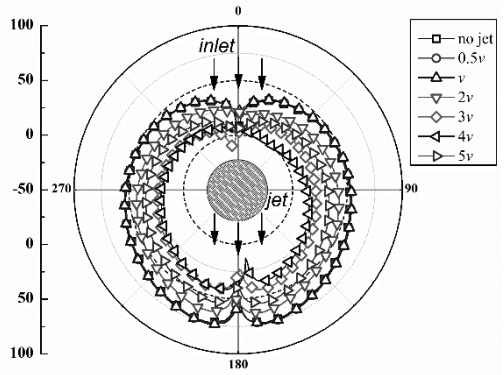

(b) Acoustic directivity of 20*d* at *Re*=3900

Fig. 12. Acoustic directivity of different *Re.*

5. CONCLUSIONS

In the present work, in order to reduce the noise radiated from flow past a blunt body, the synthetic jet is added to the backside of a circular cylinder. At first, the *PANS* model was introduced to the simulation of flow around the cylinder. After the verification of the *PANS* model, the model with lower f_k shows accuracy in comparison with the experimental value. Combining the unsteady flow information which is calculated by *PANS* model with Lighthill theory, the acoustic field was predicted.

After analysis of flow field and acoustic field, it is noted that the synthetic jet has impact action to the flow around blunt body, suppressing the vortices shedding, and altering the frequency of vortex shedding in the view of flow field. Through the alteration of flow field, the pressure fluctuation which contributes to acoustic has been reduced. So that, the sound pressure level is reduced and the directivity curve does not remain the '8' shape while the synthetic jet velocity increases.

Within these effective analyses, this research brings out a new approach to control the noise generated from flow past a circular cylinder. The synthetic jet behind the cylinder can reduce the noise through controlling the vortex shedding from the cylinder. If the synthetic jet velocity is enough, the sound pressure level can be reduced and this maybe an exciting result for naval facilities and aerospace equipment.

ACKNOWLEDGMENTS

This research is funded by the National Key Research and Development Project of China (No. SQ2019YFC140019-03), Shandong Key Research and Development Program (No. 2019JZZY010819), project ZR2020ME175 supported by Shandong Provincial Natural Science Foundation, project ZR2020QE192 supported by Shandong Provincial Natural Science Foundation and the Science and Technology Project of Qilu University of Technology (Shandong Academy of Sciences) (No. 2020QN0024). The authors especially thank the reviewer's many helpful suggestions to improve this manuscript.

REFERENCES

Anibal, M. (2018). Scale-Adaptive Simulation of Flow around a Circular Cylinder near a Plane Boundary. *Journal of Applied Fluid Mechanics* 11(6), 1477-1488.

Arwatz, G., I. Fono and A. Seifert (2012). Suction and Oscillatory Blowing Actuator. *Aiaa Journal* 46(46), 1107-1117.

Chaouat, B. (2010). Subfilter-scale transport model for hybrid RANS/LES simulations applied to a complex bounded flow. *Journal of Turbulence* 11(51), 1-30.

Davidson, L. and S. H. Peng (2013). Embedded Large-Eddy Simulation Using the Partially Averaged Navier-Stokes Model. *Aiaa Journal* 51(5), 1066-1079.

Girimaji, S. S., R. Srinivasan and E. Jeong (2003). PANS Turbulence Model for Seamless Transition Between RANS and LES: Fixed-Point Analysis and Preliminary Results. *SME/JSME Joint Fluids Summer Engineering Conference*.

Jeong, J. J. J. and F. Hussain (1995). On the identification of a vortex. *Journal of Fluid Mechanics* 332(1), 339-363.

Kou, J., C. Gao, W. Zhang and Z. Ye (2017). Active control of transonic buffet flow. *Journal of Fluid Mechanics* 824, 312-351.

Lakshmipathy, S. and S. Girimaji (2006). *Partially-averaged Navier-Stokes method for turbulent flows: K-ω model implementation.* Aiaa Aerospace Sciences Meeting & Exhibit.

Lourenco, L. M. and C. Shih (1993). Characteristics of the plane turbulent near wake of a circular cylinder. A particle image velocimetry study.

Lyu, B., A. P. Dowling and I. Naqavi (2017). Prediction of installed jet noise. *Journal of Fluid Mechanics* 811, 234-268.

Lighthill, M. J. (1954). On Sound Generated Aerodynamically. II. Turbulence as a Source of Sound. *Proceedings of the Royal Society A Mathematical Physical & Engineering Sciences*.

Shur, M., P. R. Spalart, M. Strelets and A. Travin (2011). A rapid and accurate switch from RANS to LES in boundary layers using an overlap region. *Flow Turbulence & Combustion* 86(2), 179-206.

Norberg, C. (1998). LDV-measurements in the near wake of a circular cylinder. Advances in the Understanding of Bluff Body Wakes and Vortex-Induced Vibration, *Washington, D. C.; Proc. 1998 ASME Fluids Engineering Division* (Annual Summer Meeting).

Ong, L. and J. Wallace (1996). The velocity field of the turbulent very near wake of a circular cylinder. *Experiments in Fluids* 20(6), 441-453.

Paul, M. N. and S. Tiwari (2019). On Wake Analysis of Flow Past Rotating Downstream Cylinder using Hilbert-Huang Transformation. *Journal of Applied Fluid Mechanics* 12(1), 175-186.

Rubel, A. (1985). On the vortex stretching modification of the k-epsilon turbulence model-Radial jets. *Aiaa Journal* 23(7), 1129-1130.

Samulyak, R. H. C. Chen and K. Yu (2016). Second Order Upwind Lagrangian Particle Method for Euler Equations. *Procedia Computer Science* 80, 2433-2437.

Sen, U., A. Mukhopadhyay and S. Sen (2017). Effects of fluid injection on dynamics of flow past a circular cylinder. *European Journal of Mechanics B/Fluids* 61, 187-199.

Speziale, C. G. (1997). Computing non-equilibrium turbulent flows with time-dependent rans and vles. *Lecture Notes in Physics* 490, 123-129.

Strykowski, P. J. and K. R. Sreenivasan (1990). On the formation and suppression of vortex 'shedding' at low Reynolds numbers. *Journal of Fluid Mechanics* 218, 71-107.

Wang, J. J., P. F. Zhang, S. F. Lu and K. Wu (2006). Drag Reduction of a Circular Cylinder Using an Upstream Rod. *Flow Turbulence & Combustion* 76(1), 83-101.

Wilcox, J., J. Robles, D. C. J. Marsden and P. Blowers (2003). Theoretically Predicted Rate Constants for Mercury Oxidation by Hydrogen Chloride in Coal Combustion Flue Gases. *Environmental Science & Technology* 37(18), 4199-4204.

Williams, Ffowcs, J. F. (1974). Sound production at the edge of a steady flow. *Journal of Fluid Mechanics* 66(04), 791.

Yahiaoui, T., M. Belhenniche and B. Imine (2015). Effect of Moving Surface on NACA 63218 Aerodynamic Performance. *Epj Web of Conferences*.

You, D. and P. Moin (2007). Effects of hydrophobic surfaces on the drag and lift of a circular cylinder. *Physics of Fluids* 19(8), 081701.

Zdravkovich, M. M. (1981). Review and classification of various aerodynamic and hydrodynamic means for suppressing vortex shedding. *Journal of Wind Engineering & Industrial Aerodynamics* 7(2), 145-189.